

DMD-Based Model Predictive Control for a Coupled PDE-ODE System

Dirk Wolfram* Thomas Meurer**

* Chair of Automation and Control, Faculty of Engineering, Kiel University, 24143 Kiel, Germany, e-mail: dw@tf.uni-kiel.de.

** Digital Process Engineering Group, Institute for Mechanical Process Engineering and Mechanics, Karlsruhe Institute of Technology (KIT), 76187 Karlsruhe, Germany, e-mail: thomas.meurer@kit.edu.

Abstract: Models resulting from the application of the finite element method (FEM) are usually high dimensional, thus in general preventing the application of optimal control concepts under real-time conditions. In this work a system consisting of the heat equation defined on a 3-dimensional domain with local in-domain thermal actuators is considered, whose modeling results in a coupled PDE-ODE description. Based on simulation data, a data driven reduced order model is determined using the Dynamic Mode Decomposition with control (DMDc). Based on the DMDc model a model predictive control (MPC) approach with state estimator is developed to realize a desired temperature profile on the given domain. The concept is evaluated involving the high-dimensional finite element model as plant model.

Copyright © 2023 The Authors. This is an open access article under the CC BY-NC-ND license (<https://creativecommons.org/licenses/by-nc-nd/4.0/>)

Keywords: Distributed parameter systems, Reduced order model, Data-driven control, Model predictive control, Heat conduction

1. INTRODUCTION

MPC is a well established model based control algorithm, see, e.g., Rawlings (2000), which is applied in a variety of different research fields and applications based on linear and nonlinear ordinary differential equations (ODEs), see e.g. Grüne and Pannek (2011) and partial differential equations (PDEs), see e.g. Christofides et al. (2011). Examples in PDE-constrained MPC address diffusion-convection-reaction processes, see, e.g., Meurer and Andrej (2018), nonlinear PDEs using the Koopman theory, see, e.g., Arbabi et al. (2018), applications in power generation in wind farms (Ghanavati and Chakravarthy, 2019), drug manufacturing (Grimard et al., 2021) or flow reactors (Dufour et al., 2003).

In this work, a MPC for a coupled PDE-ODE system motivated by a 3-dimensional thermal problem is designed. Due to the fact that the approximation of the coupled system using, e.g., the FE method results in a high-dimensional model, solving the optimal control (OPC) problem on a receding horizon involving a full state observer is not real-time capable. To address this, the model order has to be reduced as suggested in, e.g., Hovland et al. (2006). In contrast to classical MOR techniques such as modal truncation, Proper Orthogonal Decomposition (POD) or Balanced Proper Orthogonal Decomposition (BPOD), see, e.g., Saak et al. (2019), subsequently the numerical solution of coupled PDE-ODE system is used to generate a data basis for the model free DMDc approach, see, e.g., Brunton and Kutz (2019); Proctor et al. (2016). The Dynamic Mode Decomposition (DMD) was first introduced by Schmid (2010) in a fluid dynamics context. Recently, SINDy-MPC as a combination of the DMD with MPC has been introduced (Kaiser et al., 2017; Fasel et al.,

2021). Kaiser et al. (2017) highlight that the limitation of SINDy is the dimension of the data basis. Due to the fact, that that a desired profile on the whole domain should be achieved, the limitations of SINDy are exceeded, so that DMDc will be used.

This work is structured as follows. In Section 2 the coupled PDE-ODE system and the considered control problem are introduced. Based on the model equations and their approximation the DMDc model is computed in Section 3. The resulting low order model is the foundation for developing the state observer and the MPC in Sections 4 and 5, respectively. The observer-based MPC is evaluated numerically in Section 6.

2. SETUP AND MATHEMATICAL MODEL

The considered process is motivated by a 3-dimensional heat conduction problem. Figure 1 illustrates the $0.15\text{ m} \times 0.15\text{ m} \times 0.1\text{ m}$ aluminum block including 36 possible heat cartridge locations indicated by the bore holes. The $\mu = 8$ occupied actuator positions are highlighted in blue. The resulting mathematical model has been introduced in Wolfram and Meurer (2021), where in addition the parameter identification problem has been addressed. Subsequently a short overview is provided together with a summary of the differences.

The spatial-temporal evolution of the temperature $T(t, \mathbf{z})$ in the body Ω and on its surface Γ is captured by the linear heat equation

$$\rho c_p \frac{\partial T}{\partial t} - \nabla \cdot (\lambda \nabla T) = 0, \quad \mathbf{z} \in \Omega, \quad t > 0 \quad (1a)$$

with the initial value

$$T = T_0, \quad \mathbf{z} \in \Omega, \quad t = 0. \quad (1b)$$

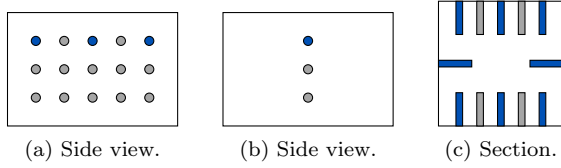


Fig. 1. Schematics of the geometry: sides views and sectional plane through one actuation layer (Wolfram and Meurer, 2021). Possible actuator locations are marked gray, used actuator locations are marked blue.

Here, ρ , c_p , and λ denote density, specific heat capacity, and heat conductivity of the solid body, respectively. Differing from Wolfram and Meurer (2021) here

$$T = T_{\text{abs}} - T_R$$

holds, so that T is the temperature difference between the absolute temperature T_{abs} of the body and the temperature of the surrounding air T_R , which is assumed constant. The heat inflow generated by each of the μ actuators is assumed to show PT₁ behavior given by the ODE

$$0 = \mathcal{S}_o \dot{\phi}_o + \phi_o - \mathcal{D}_o Q_{A,o} u_o, \quad t > 0, \quad \phi_o(0) = 0, \quad (1c)$$

with \mathcal{S}_o the time constant, $Q_{A,o}$ the maximal heat flow divided by 100 and \mathcal{D}_o the power correction parameter of the heat cartridges. The input u_o can be described as the degree of activation with

$$0 \leq u_o \leq 100, \quad \forall o \in \{1, \dots, \mu\}. \quad (1d)$$

Due to the fact that ϕ_o is a heat flow the interaction between the actuators and the solid body can be described by the inhomogeneous Neumann boundary condition (BC)

$$\mathbf{n} \cdot \lambda \nabla T = \phi_o, \quad \mathbf{z} \in \Gamma^{A,o}, \quad t > 0 \quad (1e)$$

for $o \in \{1, \dots, \mu\}$. This BC implies a uniform, but time-varying heat inflow over the actuator surface $\Gamma^{A,o} \subset \Gamma$. Assuming the bottom surface Γ^I to be insulated, the homogeneous Neumann BC

$$\mathbf{n} \cdot \lambda \nabla T = 0, \quad \mathbf{z} \in \Gamma^I, \quad t > 0 \quad (1f)$$

holds true. The remaining surfaces $\Gamma^R \subset \Gamma$ have a direct contact with the surrounding constant air temperature T_R , so that a convective heat transfer

$$\mathbf{n} \cdot \lambda \nabla T = -h_R T, \quad \mathbf{z} \in \Gamma^R, \quad t > 0, \quad (1g)$$

with the heat transfer coefficient h_R , exists.

Eight thermocouples are included to measure the temperature at the positions $\mathbf{z}_{\text{PM},l}$, $l \in \{1, \dots, \xi\}$, with $\xi = 8$. Their locations are summarized Tab. 1 using a body fixed coordinate system placed in the center of the solid body. Their spatial characteristics is described by $c_{\Gamma,l} \in L_2(\Gamma)$, so that the output value can be determined using

$$y_{\Gamma,l} = \int_{\Gamma} c_{\Gamma,l} T \, d\Gamma, \quad l = 1, \dots, \xi. \quad (2)$$

The system parameters of the coupled PDE-ODE system (1) are listed in Tab. 2.

Table 1. Sensor positions.

Sensor	1	2	3	4	5	6	7	8
z_1 in m	-0.05	0.00	0.05	0.05	0.05	0.00	-0.05	-0.05
z_2 in m	0.05	0.05	0.05	0.05	0.05	0.05	0.05	0.05
z_3 in m	0.05	0.05	0.05	0.00	-0.05	-0.05	-0.05	0.00

In order to approximate the solution to the PDE open source finite element (FE) code `firedrake` is used, see, e.g., Rathgeber et al. (2016); Firedrake (2021). The FEM

requires the weak formulation of (1a), which can be obtained by multiplying the equation with the test function $v \in H^1(\Omega)$ and integrating over the domain Ω

$$0 = \int_{\Omega} v \rho c_p \frac{\partial T}{\partial t} \, d\Omega - \int_{\Omega} v \nabla \cdot (\lambda \nabla T) \, d\Omega.$$

Applying Green's first identity and inserting the boundary conditions (1e)-(1g) the weak form reads

$$0 = \int_{\Omega} v \rho c_p \frac{\partial T}{\partial t} \, d\Omega + \int_{\Omega} \lambda (\nabla T \cdot \nabla v) \, d\Omega - \int_{\Gamma^R} v h_R (T_R - T) \, d\Gamma^R - \sum_{o=1}^{\mu} \int_{\Gamma^{A,o}} v \phi_o \, d\Gamma^{A,o}.$$

The FEM requires the local discretization of the geometry, which is achieved by using the meshing tool `trellis Pro` (Version 16.5) with tetrahedral elements. The resulting mesh, consisting of 558732 tetrahedrals and $\sigma = 98989$ nodes, is shown in Fig. 2. The resulting system is given by

$$\mathbf{0} = \begin{bmatrix} M & 0 \\ 0 & \mathcal{S} \end{bmatrix} \begin{bmatrix} \dot{\mathbf{T}}(t) \\ \dot{\boldsymbol{\phi}}(t) \end{bmatrix} + \begin{bmatrix} K & H \\ 0 & I \end{bmatrix} \begin{bmatrix} \mathbf{T}(t) \\ \boldsymbol{\phi}(t) \end{bmatrix} + \begin{bmatrix} 0 \\ \mathcal{X} \end{bmatrix} \mathbf{u}(t), \quad (3a)$$

for $t > 0$, $[\mathbf{T}(0) \ \boldsymbol{\phi}(0)]^T = [\mathbf{T}_0 \ \boldsymbol{\phi}_0]^T$, with $\mathcal{X} = \text{diag}(-\mathcal{D}_1 Q_{A,1}, \dots, -\mathcal{D}_{\mu} Q_{A,\mu})$ and $\mathcal{S} = \text{diag}(\mathcal{S}_1, \dots, \mathcal{S}_{\mu})$. The first set of ODEs refers to the discretized PDE with the node temperatures $\mathbf{T}(t)$ as state variable, whereas the second set of equations represents the actuator dynamics. The discretized output equation reads

$$\mathbf{y}(t) = [G \ 0] \begin{bmatrix} \mathbf{T}(t) \\ \boldsymbol{\phi}(t) \end{bmatrix} \quad (3b)$$

Based on the solution of this coupled ODE system the data basis for the DMDC algorithm is determined.

3. DYNAMIC MODE DECOMPOSITION

The DMDC is a model free approach for determining a state space model using only data matrices Schmid (2010). To address the inhomogeneous case with external input the DMDC following Proctor et al. (2016) is considered.

It is assumed, that the temperature can be described by the discrete time system

$$\mathbf{T}_{k+1} \approx \hat{A} \mathbf{T}_k + \hat{B} \mathbf{u}_k, \quad \mathbf{k} \in \mathbb{N} \cup \{0\},$$

where \mathbf{T}_0 is the initial state, \mathbf{T}_k is a snapshot of the temperature $\mathbf{T}(t)$ at the time $t = \mathbf{k}\Delta t$, \mathbf{u}_k is a snapshot of the input $\mathbf{u}(t)$ and $\hat{A} \in \mathbb{R}^{\sigma \times \sigma}$ as well as $\hat{B} \in \mathbb{R}^{\sigma \times \mu}$ are unknown matrices. The DMDC uses the snapshot matrix

$$X = [\mathbf{T}_0 \ \mathbf{T}_1 \ \dots \ \mathbf{T}_{M-1}], \quad (4a)$$

containing M snapshots of the temperature, its time shifted version

$$X' = [\mathbf{T}_1 \ \mathbf{T}_1 \ \dots \ \mathbf{T}_M] \quad (4b)$$

and the related input values

$$\boldsymbol{\gamma} = [\mathbf{u}_0 \ \mathbf{u}_1 \ \dots \ \mathbf{u}_{M-1}] \quad (4c)$$

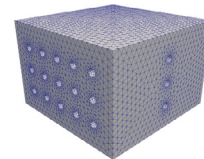


Fig. 2. Meshed body.

Table 2. Physical parameters.

Para.	ρ	c_p	λ	h_R	D_1	D_2	D_3	$D_{4,5}$	D_6	D_7	D_8	$S_{1,2,6,7,8}$	$S_{3,4,5}$
Value	2700.0	921.0	209.919	7.588	0.62	0.8	0.92	1.01	0.8	0.65	1.44	1.001	1.002
Unit	kg m^{-3}	$\text{kg m}^2 \text{s}^{-2} \text{K}^{-1}$	$\text{W m}^{-1} \text{K}^{-1}$	$\text{W m}^{-2} \text{K}^{-1}$	–	–	–	–	–	–	–	s	s

for solving the singular value decompositions (SVDs) and truncating the singular values after α singular values of the input space

$$\begin{bmatrix} X \\ \gamma \end{bmatrix} \approx \tilde{U} \tilde{\Sigma} \tilde{V}^*$$

and of the output space

$$X' \approx \hat{U} \hat{\Sigma} \hat{V}^*$$

using the truncation order $\nu < \alpha \ll \sigma$. The reduced order system

$$\mathbf{s}_{k+1} = A \mathbf{s}_k + B \mathbf{u}_k, \quad (5)$$

with initial state $\mathbf{s}_0 \in \mathbb{R}^\nu$, $A \in \mathbb{R}^{\nu \times \nu}$, and $B \in \mathbb{R}^{\nu \times \mu}$ is then obtained with

$$A = \hat{U}^* X' \tilde{V} \tilde{\Sigma}^{-1} \tilde{U}_1^* \hat{U}, \quad B = \hat{U}^* X' \tilde{V} \tilde{\Sigma}^{-1} \tilde{U}_2^*.$$

Here, the matrices $\tilde{U}_1 \in \mathbb{R}^{\sigma \times \alpha}$ and $\tilde{U}_2 \in \mathbb{R}^{\mu \times \alpha}$ are the data and input related parts of the truncated input space SVD, i.e., $\tilde{U}^* = [\tilde{U}_1^* \quad \tilde{U}_2^*]$. The relation between the snapshots and the DMDc generated states is described by

$$\mathbf{T}_k = \hat{U} \mathbf{s}_k, \quad (6)$$

with $\hat{U} \in \mathbb{R}^{\sigma \times \nu}$. Applying this transformation the output (3b) can be expressed in the new states

$$\mathbf{y}_k = G \hat{U} \mathbf{s}_k = C \mathbf{s}_k, \quad (7)$$

note that $\phi(t)$ has no influence to the output and can be neglected.

To generate the snapshot matrix system (3a) is solved using an implicit Euler integration scheme with sampling time $\Delta t = 0.2$ s. To generate a data basis capturing a wide range of different inputs the applied external signals are composed of a combination of piecewise constant and trigonometric functions, see Fig. 3.

Remark 1. Note that the input \mathbf{u}_k is used for the snapshots, so that a model between the degree of activation and the temperature results from the DMDc.

The truncation order of the SVDs in the DMDc algorithm is chosen as 0.00001% of the maximal singular value in each SVD, resulting in $\nu = 28$ states. For evaluating the quality of the resulting model the root mean square error (RMSE) is used

$$|\Delta e_k| = \sqrt{\frac{\|e_k\|_{L_2}}{\mathcal{V}(\Omega)}}, \quad (8)$$

with $\|e_k\|_{L_2}$ referring to the L_2 -Norm of the error $e_k = \mathbf{T}_k - \hat{U} \mathbf{s}_k$ and $\mathcal{V}(\Omega)$ referring to the volume of the domain, see, e.g., Zienkiewicz et al. (2005). It can be interpreted as a mesh adjusted mean error over the whole domain. Figure 4 (blue curve) shows the resulting RMSE for the excitation using the same input signal for the generation of the reduced order model and the evaluation. The RMSE remains below 0.02 K. After the dynamic input change ($t = 500$ s) the input is constant at 80% of the maximum input until $t = 750$ s. During this period the RMSE rises to its maximum value at approximately 0.0187 K, whereas

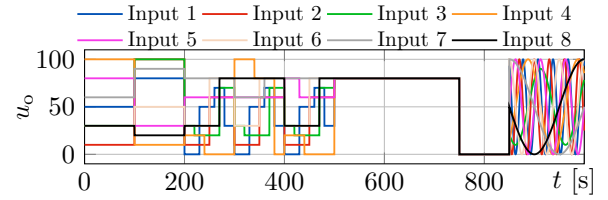


Fig. 3. Input for generating the DMDc data basis.

the actuator power drops to 0. Taking the whole signal into account, the maximum error values occur at rapid input changes. For evaluating the DMDc a different input, shown in Fig. 5, is applied to the PDE and the reduced order DMDc model. In this case a longer constant input is applied to the actuators, although all actuators are excited with a different gain. The resulting RMSE is also shown in Fig. 4 (red curve). During the dynamic input change, the error is slightly larger compared to the generation signal. The error rises to 0.04 K when the input is constant with a different value in each actuator and decreases when the input is constant at 80% of the maximum input power. Figure 6 shows the RMSE in relation to the root mean square (RMS) temperature of the structure. The RMS temperature can be interpreted as the mean temperature of the structure, obtained by replacing the error in (8) with the solution of the full order model \mathbf{T}_k . After 10 s the error for the generation and validation input falls below 1%. During the remaining heating process 0.5% relative error is not exceeded.

Based on these evaluations it is concluded that the generated DMDc model is a valid representation of the full order model and is hence used for designing a state observer.

4. DMD-BASED KALMAN FILTER DESIGN

For designing a MPC knowledge of the full state of (5) is required. In order to estimate the states using the measurements a discrete time Kalman filter is set up. Following, e.g., Lewis et al. (2008) the Kalman filter assumes a discrete system of the form

$$\begin{aligned} \mathbf{s}_{k+1} &= A \mathbf{s}_k + B \mathbf{u}_k + \boldsymbol{\kappa}_k \\ \mathbf{y}_k &= C \mathbf{s}_k + \boldsymbol{\chi}_k, \end{aligned}$$

with the initial state \mathbf{s}_0 , the process noise $\boldsymbol{\kappa}_k \in \mathbb{R}^\nu$ and the measurement noise $\boldsymbol{\chi}_k \in \mathbb{R}^\xi$. Process and measurement noise are assumed to be white noise processes with zero mean value and covariance matrices $\mathcal{Q} \in \mathbb{R}^{\nu \times \nu}$ and $\mathcal{R} \in \mathbb{R}^{\xi \times \xi}$, respectively. Taking into account that the

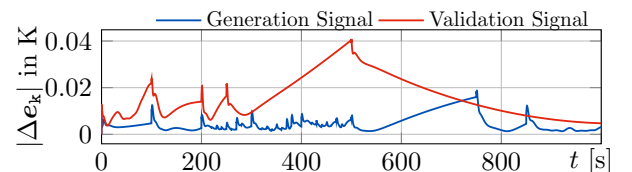


Fig. 4. RMSE between the PDE simulation data basis and its reduced order representation.

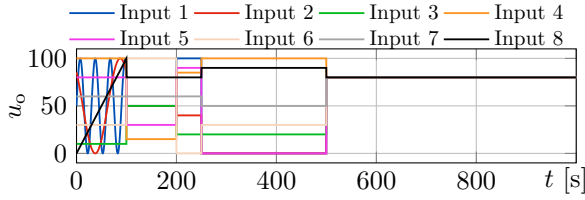


Fig. 5. Input for validating the reduced order model.

underlying system equations are linear and time invariant a constant observer gain $L = APC^T(CPC^T + \mathcal{R})$ can be determined by solving the discrete algebraic matrix Riccati equation $P = APA^T + Q - APC^T(CPC + \mathcal{R})^{-1} + CPA^T$. Using the determined filter gain the resulting state estimator reads

$$\hat{\mathbf{s}}_{k+1} = A\hat{\mathbf{s}}_k + B\mathbf{u}_k + L(\mathbf{y}_k - \hat{\mathbf{y}}_k) \quad (9a)$$

$$\hat{\mathbf{y}}_k = C\hat{\mathbf{s}}_k, \quad (9b)$$

with the initial state $\hat{\mathbf{s}}_0$.

Remark 2. Note that by transforming the states of the state estimator $\hat{\mathbf{s}}_k$ back, using $\hat{\mathbf{T}}_k = \hat{U}\hat{\mathbf{s}}_k$, an estimation of the temperature distribution is obtained.

5. DISCRETE TIME MPC

To robustly achieve a desired temperature profile an MPC is designed based on the determined process model (5), (7). The MPC can be interpreted as a feedforward control computer for the next \mathcal{C} time steps (the control horizon) based on the prediction over \mathcal{P} time steps (the prediction horizon) before repeating the solution process sequentially. Herein the observer (9) is used to update the state information for each receding horizon.

The design of the discrete time MPC follows the lines of, e.g., Wang (2009); Rosenzweig et al. (2018); Kater (2019) and relies on rewriting (5), (7) as an augmented model. The constrained optimization problem is solved using a primal-dual-method using Hildreth's quadratic programming procedure, see Wang (2009). Let

$$\mathbf{w}_k = Z\mathbf{s}_k \quad (10)$$

denote the control variable, which is supposed to follow a desired output. Depending on $Z \in \mathbb{R}^{\kappa \times \sigma}$ this enables us also to impose a certain temperature profile, at least approximately. Note that \mathbf{w}_k may be independent from the measured outputs \mathbf{y}_k .

By building the difference between the current and previous state $\Delta\mathbf{s}_k = \mathbf{s}_k - \mathbf{s}_{k-1}$ as well as the input difference $\Delta\mathbf{u}_k = \mathbf{u}_k - \mathbf{u}_{k-1}$ the change of the discrete model (5) in each time step can be expressed as

$$\Delta\mathbf{s}_{k+1} = A\Delta\mathbf{s}_k + B\Delta\mathbf{u}_k. \quad (11)$$

To connect (10) to $\Delta\mathbf{s}_k$ the difference $\mathbf{w}_{k+1} - \mathbf{w}_k$ is used and rearranged to

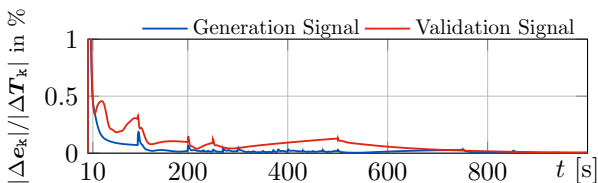


Fig. 6. Relative RMSE with respect to RMS temperature.

$$\mathbf{w}_{k+1} = \mathbf{w}_k + Z\Delta\mathbf{s}_{k+1}.$$

By introducing the augmented state $\mathbf{s}_k^A = [\Delta\mathbf{s}_k^T, \mathbf{w}_k^T]^T$ the augmented model is derived

$$\mathbf{s}_{k+1}^A = \mathcal{A}\mathbf{s}_k^A + \mathcal{B}\Delta\mathbf{u}_k \quad (12a)$$

$$\mathbf{w}_k = Z\mathbf{s}_k^A, \quad (12b)$$

where

$$\mathcal{A} = \begin{bmatrix} A & 0 \\ ZA & I \end{bmatrix}, \quad \mathcal{B} = \begin{bmatrix} B \\ ZB \end{bmatrix}, \quad Z = [0 \ I].$$

The input to the augmented model can be described as the change of the actuator degree of activation and enables us to restrict the rate of input changes. The new structure introduces an integral like behavior regarding the output in the closed-loop system, see Kater (2019). Note that $\Delta\mathbf{s}_0$ depends on the undefined state \mathbf{s}_{-1} , so that $\mathbf{s}_k^A = [0, \mathbf{w}_0]$ is assumed.

For determining the control input the MPC requires the prediction of the next \mathcal{P} time steps

$$W = [\mathbf{w}_{k+1,k}^T, \mathbf{w}_{k+2,k}^T, \dots, \mathbf{w}_{k+\mathcal{P},k}^T]^T$$

depending on a given set of inputs

$$\Delta\Psi = [\Delta\mathbf{u}_k^T, \Delta\mathbf{u}_{k+1}^T, \dots, \Delta\mathbf{u}_{k+\mathcal{P}-1}^T]^T.$$

Here $\mathbf{w}_{k+i,k}$ describes the prediction of the i th output with respect to the current state \mathbf{s}_k^A . Using

$$\mathbf{s}_{k+i}^A = \mathcal{A}^i\mathbf{s}_k^A + \sum_{j=0}^{i-1} \mathcal{A}^{i-1-j}\mathcal{B}\Delta\mathbf{u}_{k+j}$$

the matrix W can be determined by

$$W = F\mathbf{s}_k^A + \Phi\Delta\Psi \quad (13)$$

with

$$F = \begin{bmatrix} Z\mathcal{A} \\ Z\mathcal{A}^2 \\ \vdots \\ Z\mathcal{A}^{\mathcal{P}} \end{bmatrix}, \quad \Phi = \begin{bmatrix} Z\mathcal{B} & 0 & \dots & 0 \\ Z\mathcal{A}\mathcal{B} & Z\mathcal{B} & \dots & 0 \\ \vdots & \vdots & \ddots & \vdots \\ Z\mathcal{A}^{\mathcal{P}-1}\mathcal{B} & Z\mathcal{A}^{\mathcal{P}-2}\mathcal{B} & \dots & Z\mathcal{B} \end{bmatrix}.$$

Due to the fact that the state \mathbf{s}_k^A is not known during the MPC calculation the observed state $\hat{\mathbf{s}}_k^A$ has to be used.

In order to find the optimal input trajectory Ψ for minimizing the error between the predicted output W and the reference trajectory

$$W^* = [(\mathbf{w}_{k+1}^*)^T, (\mathbf{w}_{k+2}^*)^T, \dots, (\mathbf{w}_{k+\mathcal{P}}^*)^T]^T$$

the discrete optimization problem

$$\min_{\Delta\Psi} \mathfrak{J} = (W^* - W)^T Q (W^* - W) + \Delta\Psi^T R \Delta\Psi \quad (14a)$$

with the symmetric and positive definite weighting matrix $Q \in \mathbb{R}^{\kappa\mathcal{P} \times \kappa\mathcal{P}}$ as well as the symmetric and positive semi-definite matrix $R \in \mathbb{R}^{\mu\mathcal{P} \times \mu\mathcal{P}}$ subject to constraints on the input as well as the rate of change of the input

$$\underline{\Psi} \leq \Psi \leq \overline{\Psi} \quad (14b)$$

$$\underline{\Delta\Psi} \leq \Delta\Psi \leq \overline{\Delta\Psi}. \quad (14c)$$

Here $\Psi = \mathbf{u}_{k-1} + \Delta\Psi$ contains the next \mathcal{P} input vectors starting with \mathbf{u}_k , $\underline{\Psi}$ and $\overline{\Psi}$ are lower and upper bounds for the input, and $\underline{\Delta\Psi}$, $\overline{\Delta\Psi}$ are bounds on the rate. Inserting (13) into the cost function (14a) can be rewritten as a quadratic problem for the input $\Delta\Psi$, i.e., $\mathfrak{J} = \frac{1}{2}\Delta\Psi^T H \Delta\Psi + \Delta\Psi^T \mathbf{f} + \beta^T Q \beta$, where $\beta = W^* - F\hat{\mathbf{s}}_k^A$, $H = 2(\Phi^T Q \Phi + R)$ is a symmetric matrix and $\mathbf{f} = -2\Phi^T Q \beta$. Note that $\beta^T Q \beta$ is constant (with respect to $\Delta\Psi$) and has

no influence on the solution, so that the term is neglected. The minimization of this unconstrained cost function is obtained by $\Delta\Psi_{nc} = -H^{-1}\mathbf{f}$.

In order to determine the constrained solution the input constraints (14b) have to be reformulated in terms of the input change. Since $\Delta\mathbf{u}_k$ contains the change of the input from \mathbf{u}_{k-1} , each input between the time steps k and $k + \mathcal{P} - 1$ can be described as the sum of input changes

$$\Psi = \mathcal{G}_1\mathbf{u}_{k-1} + \mathcal{G}_2\Delta\Psi, \quad (15)$$

where $\mathcal{G}_1 = [\mathbf{I}, \mathbf{I}, \dots, \mathbf{I}]^T \in \mathbb{R}^{\mu\mathcal{P} \times \mu}$ contains \mathcal{P} μ -dimensional identity matrices \mathbf{I} and

$$\mathcal{G}_2 = \begin{bmatrix} \mathbf{I} & 0 & \dots & 0 \\ \vdots & \vdots & \ddots & \vdots \\ \mathbf{I} & \mathbf{I} & \dots & \mathbf{I} \end{bmatrix} \in \mathbb{R}^{\mu\mathcal{P} \times \mu\mathcal{P}}.$$

With this the input constraint (14b) can be reformulated in terms of two inequality constraints $\mathcal{G}_2\Delta\Psi \leq \overline{\Psi} - \mathcal{G}_1\mathbf{u}_{k-1}$ and $-\mathcal{G}_2\Delta\Psi \leq -\underline{\Psi} + \mathcal{G}_1\mathbf{u}_{k-1}$. Thus taking into account (14c) the set of constraints read

$$\Xi\Delta\Psi \leq \xi, \quad (16)$$

with $\Delta\Psi = [\mathcal{G}_2^T, -\mathcal{G}_2^T, \mathbf{I}, -\mathbf{I}]^T$ and

$$\xi = [(\overline{\Psi} - \mathcal{G}_1\mathbf{u}_{k-1})^T, (-\underline{\Psi} + \mathcal{G}_1\mathbf{u}_{k-1})^T, \overline{\Delta\Psi}^T, -\underline{\Delta\Psi}^T]^T.$$

Considering the extended cost function

$$\mathfrak{J} = \frac{1}{2}\Delta\Psi^T H \Delta\Psi + \Delta\Psi^T \mathbf{f} + \boldsymbol{\lambda}^T (\Xi\Delta\Psi - \xi),$$

involving the Lagrange multipliers $\boldsymbol{\lambda}$ the Karush-Kuhn-Tucker (KKT) conditions can be determined

$$\begin{aligned} H\Delta\Psi + \mathbf{f} + \Xi^T \boldsymbol{\lambda} &= 0 \\ \boldsymbol{\lambda}^T (\Xi\Delta\Psi - \xi) &= 0, \quad \boldsymbol{\lambda} \geq 0. \end{aligned} \quad (17)$$

Here, the first equation describes the gradient of the cost function with respect to the input change and the second refers to the complementary slackness condition.

For the numerical solution a primal-dual-method is used, so that the Lagrange multipliers are determined by formulating a dual problem, whose solution is used to compute $\Delta\Psi$. The primal problem reads

$$\max_{\boldsymbol{\lambda} \geq 0} \min_{\Delta\Psi} \frac{1}{2}\Delta\Psi^T H \Delta\Psi + \Delta\Psi^T \mathbf{f} + \boldsymbol{\lambda}^T (\Xi\Delta\Psi - \xi). \quad (18)$$

The inner minimization problem implies

$$\Delta\Psi = -H^{-1}(\mathbf{f} + \Xi^T \boldsymbol{\lambda}). \quad (19)$$

Inserting this solution into the primal problem results in the dual problem

$$\min_{\boldsymbol{\lambda} \geq 0} \frac{1}{2}\boldsymbol{\lambda}^T K \boldsymbol{\lambda} + \boldsymbol{\lambda}^T \mathbf{v} + \frac{1}{2}\mathbf{f}^T H^{-1} \mathbf{f}, \quad (20)$$

where $K = \Xi H^{-1} \Xi^T$ and $\mathbf{v} = \Xi H^{-1} \mathbf{f} + \xi$. Referring to Wang (2009) the dual problem can be solved by using, e.g., Hildreth's quadratic programming procedure, which determines the Lagrange multipliers iteratively for $j \leq j_{\max}$. The i th element of $\boldsymbol{\lambda}$ in the j th iteration can be determined by

$$\lambda_i^j = \max(0, a_i^j) \quad (21a)$$

with

$$a_i^j = -\frac{1}{K_{ii}} \left(v_i + \sum_{m=1}^{i-1} K_{im} \lambda_m^j + \sum_{m=i+1}^{\kappa} K_{im} \lambda_m^{j-1} \right), \quad (21b)$$

where $\kappa = 4\mathcal{P}\mu$ is the number of constraints. Since λ_i^j can either be zero or positive the set of active constraints is

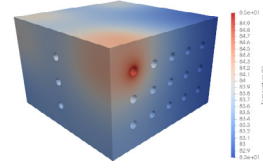


Fig. 7. Desired profile to be reached by MPC.

determined automatically. The technique converges to a desired accuracy by fulfilling $(\boldsymbol{\lambda}^j - \boldsymbol{\lambda}^{j-1})^T (\boldsymbol{\lambda}^j - \boldsymbol{\lambda}^{j-1}) < \nu$ or reaches the maximal number of iterations j_{\max} , which results in a near optimal solution. Due to the fact that this is a matrix inversion free algorithm, the computation can be continued and does not interrupt when a constraint conflict arises during the process. Based on this features the algorithm is capable of recovering from ill-conditioned constraint problems and hence is a suitable for real-time applications, see Wang (2009). Although the solution for the Lagrange multipliers can be sub-optimal, its values are only zero or positive, so that the required input change is determined by inserting the resulting Lagrange multipliers into (19). To improve convergence a warm start is considered, where the Lagrange multipliers of the last MPC iteration are used as the initial values for the new calculation (Lam et al., 2020). The optimal input for the prediction horizon \mathcal{P} is determined by inserting the input change $\Delta\Psi$ into (15). After \mathcal{C} time steps the MPC algorithm is updated using the current observer state as initial state.

6. SIMULATION RESULTS

For the evaluation the DMD-based MPC is applied to the full order FE approximation (3) of the coupled ODE system (1). Time integration is realized using an implicit Euler scheme. In order to achieve a desired profile on the whole structure all reduced order states are used for the MPC, so that the matrix Z is equal to the identity matrix of order ν . The desired profile should be a steady state solution for the coupled system (3), therefore the steady state solution for the node temperatures $\mathbf{T}_\infty = K^{-1} H \boldsymbol{\chi} \bar{\mathbf{u}}$ is determined and transformed in the DMDc states $\mathbf{w}_{k+i}^* = \hat{U}^* \mathbf{T}_\infty$, for all $i \in \{1, \dots, \mathcal{P}\}$. In this work the input $\bar{\mathbf{u}} = [20 \ 0 \ 20 \ 0 \ 30 \ 0 \ 0 \ 0]^T$ will be used, which results in the steady state profile shown in Fig. 7, with the root mean square temperature $|\Delta\mathbf{T}_k| = 83.44$ K.

For the simulation the initial state and so the initial measurement of the plant model is equal to the temperature of the surrounding air. The observer is assumed to have an initial state representing 2K above the air temperature. For the Kalman filter the covariance matrices are assigned as $\mathcal{Q} = 10\mathbf{I}$ and $\mathcal{R} = \mathbf{I}$. The cost function (14a) is parametrized using $Q = \mathbf{I}$ and $R = 300\mathbf{I}$. The upper and lower limits for inputs read $\underline{\Psi}_o = 0$ and $\overline{\Psi}_o = 100$ corresponding to minimal and maximal degree of activation. The input rates are limited to 3% of the actuator power in each sampling step resulting in $\overline{\Delta\Psi}_o = 3$ and $\underline{\Delta\Psi}_o = -3$. The parameters for Hildreth's quadratic programming procedure are assigned as $j_{\max} = 2000$ and $\nu = 10^{-4}$.

For validating the algorithm the temperature of the surrounding air is assumed to drop about 30 K at $t = 850$ s. The influence of this disturbance is not implemented in the

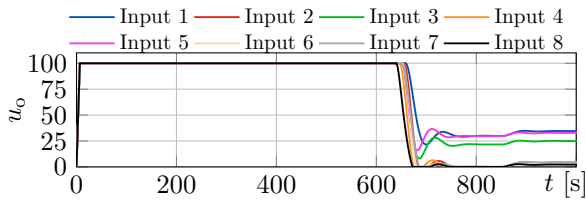


Fig. 8. Input values applied to the full order system.

DMDc model and is not provided to the MPC algorithm. The input generated by the MPC is shown in Fig. 8. The root mean squared error between the desired state and the block temperatures for the entire structure is shown in Fig. 9 and decreases below 0.01 K after 800s. During the heating process the maximal power is applied to all actuators, whereas the MPC algorithm reduces the input power between 600s and 700s for each actuator. Analogously to the generation of the desired profile the actuators 1, 3 and 5 stay active. The remaining actuators remain zero, after they regain a bit of heating power at 720s. When the disturbance appears at 850s the algorithm increases the input powers directly. Despite the error of 30 K in the air temperature, the algorithm is able to keep the RMSE below 0.12 K.

7. CONCLUSIONS

In this paper a data-driven reduced order model is derived using DMDc based on simulation data from the given full order coupled PDE-ODE system describing the temperature evolution in a 3-dimensional heating process. The resulting DMDc model with 28 states is validated with respect to the original high-dimensional FE approximation with 98997 states. Based on the reduced order model a discrete time MPC combined with a Kalman filter are derived and successfully evaluated by applying the algorithms to the full order model.

Current work addresses the application of the concept to an experimental setup as described in Wolfram and Meurer (2021) and the extension to trajectory tracking taking into account the dynamics of coupled PDE-ODE system.

REFERENCES

- Arbabi, H., Korda, M., and Mezić, I. (2018). A Data-Driven Koopman Model Predictive Control Framework for Nonlinear Partial Differential Equations. In *2018 IEEE CDC*.
- Brunton, S.L. and Kutz, J.N. (2019). *Data-Driven Science and Engineering: Machine Learning, Dynamical Systems, and Control*. Cambridge University Press.
- Christofides, P.D., Liu, J., and de la Pea, D.M. (2011). *Networked and Distributed Predictive Control: Methods and Nonlinear Process Network Applications*. Springer Publishing Company, Incorporated, 1st edition.

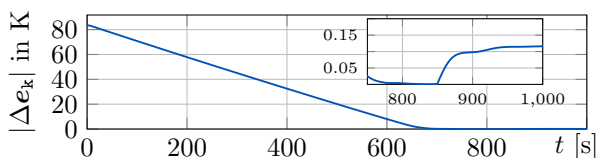


Fig. 9. RMSE with respect to the desired profile.

- Dufour, P., Couenne, F., and Toure, Y. (2003). Model predictive control of a catalytic reverse flow reactor. *IEEE Trans. on Control Systems Technology*.
- Fasel, U., Kaiser, E., et al. (2021). SINDy with Control: A Tutorial. In *2021 IEEE CDC*.
- Firedrake (2021). Software used in 'parameter identification for a 3D heating process using the adjoint method'. <https://doi.org/10.5281/zenodo.4564315>.
- Ghanavati, M. and Chakravarthy, A. (2019). PDE-Based Modeling and Control for Power Generation Management of Wind Farms. *IEEE Trans. Sustainable Energy*.
- Grimard, J., Dewasme, L., and Wouwer, A.V. (2021). Dynamic Model Reduction and Predictive Control of Hot-Melt Extrusion Applied to Drug Manufacturing. *IEEE Trans. on Control Systems Technology*.
- Grüne, L. and Pannek, J. (2011). *Nonlinear Model Predictive Control: Theory and Algorithms*. Communications and Control Engineering. Springer London.
- Hovland, S., Willcox, K., and Gravdahl, J.T. (2006). MPC for Large-Scale Systems via Model Reduction and Multiparametric Quadratic Programming. In *2006 IEEE CDC*.
- Kaiser, E., Kutz, J., and Brunton, S. (2017). Sparse identification of nonlinear dynamics for model predictive control in the low-data limit. *Proc. R. Soc. A: Mathematical, Physical and Engineering Science*.
- Kater, A. (2019). *Mathematical Modeling, Motion Planning and Control of Elastic Structures with Piezoelectric Elements*. Ph.D. thesis, Kiel University.
- Lam, V., Sattar, A., et al. (2020). Fast Hildreth-based Model Predictive Control of Roll Angle for a Fixed-Wing UAV. *IFAC-PapersOnLine*.
- Lewis, F.L., Xie, Lihua, and Popa, Dan (2008). *Optimal and Robust Estimation: With an Introduction to Stochastic Control Theory*, volume 2. CRC Press.
- Meurer, T. and Andrej, J. (2018). Flatness-based model predictive control of linear diffusion-convection-reaction processes. In *2018 IEEE CDC*.
- Proctor, J.L., Brunton, S.L., and Kutz, J.N. (2016). Dynamic mode decomposition with control. *SIAM J. on Applied Dynamical Systems*.
- Rathgeber, F., Ham, D.A., et al. (2016). Firedrake: Automating the finite element method by composing abstractions. *ACM Trans. Math. Softw.*
- Rawlings, J. (2000). Tutorial overview of model predictive control. *IEEE Control Systems Magazine*.
- Rosenzweig, P., Kater, A., and Meurer, T. (2018). Model predictive control of piezo-actuated structures using reduced order models. *Control Eng. Pract.*, 80.
- Saak, J., Siebelts, D., and Werner, S.W.R. (2019). A comparison of second-order model order reduction methods for an artificial fishtail. *Automatisierungstechnik*.
- Schmid, P.J. (2010). Dynamic mode decomposition of numerical and experimental data. *J. of Fluid Mechanics*.
- Wang, L. (2009). *Model Predictive Control System Design and Implementation Using MATLAB*. Springer Publishing Company, Incorporated, 1st edition.
- Wolfram, D. and Meurer, T. (2021). Parameter identification for a 3D heating process by the adjoint method based on experimental data. *IFAC-PapersOnLine*.
- Zienkiewicz, O., Taylor, R., and Zhu, J. (2005). *The Finite Element Method: Its Basis and Fundamentals*. Elsevier, sixth edition.